Chapter 6: Performance Improvement Studies of Gyro-twystron Using an Intermediate Cavity

6.1   Introduction

6.2   Design Methodology

    6.2.1   Magnetron Injection Gun (MIG)

    6.2.2   RF Interaction Structure

    6.2.3   Particle Collector

6.3   Beam Wave Interaction Study

    6.3.1   Modelling and Cold Simulation

    6.3.2   PIC Simulation and Validation

6.4   Conclusion

6.1   Introduction

The gyro-twystron amplifiers deliver kW to MW of RF output power at a higher frequency $\geq$ 10 GHz and become a possible candidate for RF driver and particle acceleration in addition to RADAR applications [32], [52]. The initial experiments at the University of Maryland suggested that gyro-amplifiers can deliver tenths of MW RF output power in X- and Ku-band frequency as compared to their slow-wave counterparts. The state of the art of gyro-amplifiers, including gyro-twystron, is discussed by Granatstein *et al.* and the performance of various tubes (gyroklystron and gyro-twystron) is evaluated by P/λ^2 [32]. The high power handling capabilities of the travelling wave section make gyro-twystron as a preferable gyro-amplifier for MW class operation.

The theoretical and experimental studies of the multi-cavity configuration of gyroklystron and gyro-twystron predicted the significant improvement of performance metrics. In 1985, Chu *et al.* developed the design methodology of the MW-class four cavity gyroklystron, and later Tantawi *et al.* have designed and developed the three cavity gyroklystron and further its performance metrics are investigated [38]. In the chapter, 3, 4 the multimode studies of single cavity gyro-twystron predicted an RF power of 20 MW in TE_{01} mode and its performance is limited by second harmonic TE_{02} mode. Multi cavity MW-class gyroklystron research motivates an introduction of an intermediate cavity to single cavity gyro-twystron to enhance the performance metrics.

In this Chapter, an intermediate cavity is introduced to a single cavity gyro-twystron configuration to improve the performance metrics. In section 6.2, the design methodology of gyro-twystron is discussed with the design and simulation of particle emitter and collector. In section 6.3, PIC simulation and its validation are discussed before the conclusion has been drawn in section 6.4.
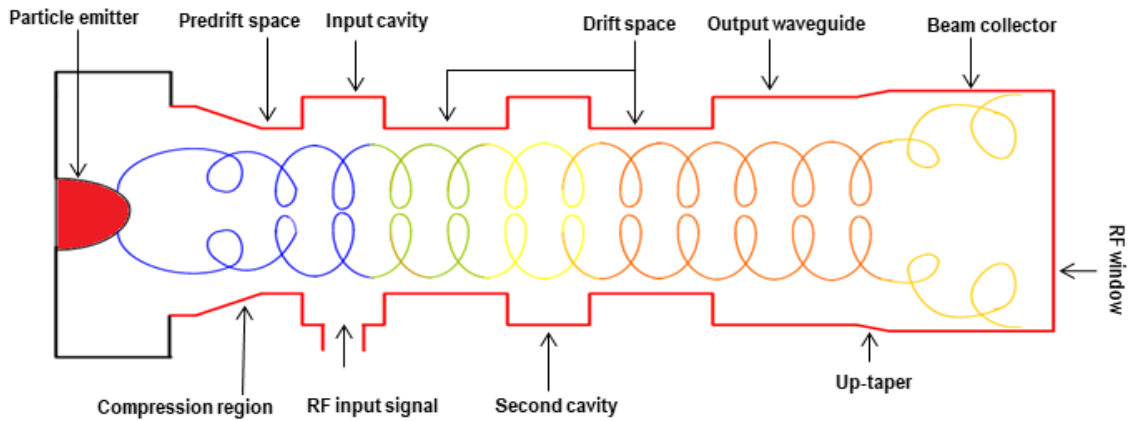
Figure 6.1 Schematic of two cavity gyro-twystron

6.2 Design Methodology

In this section, the design methodology of two cavity gyro-twystron is discussed and to enhance the performance of gyro-twystron, the particle emitter and collector are designed and optimised. Apart from the beam-wave interaction mechanism in RF interaction structure, the efficiency of gyro-twystron is primarily dependent on quality of electron beam generated by the MIG and energy extraction from the unspent particle at particle collector. The schematic of the two cavity gyro-twystron is shown in figure 6.1.

6.2.1 Magnetron Injection Gun (MIG)

The performance of gyrotron devices depends upon the quality of electron beam power. The efficiency of gyrotron devices is increasing with the pitch factor (beam velocity). However, at high value of pitch factor the velocity spread increases. This limits the Doppler upshifted operation, hence limits the bandwidth. The pitch factor and beam current are decisive parameters to achieve the stable operation of gyro amplifiers as well as start oscillation condition of gyrotron. The beam voltage and current should follow the inequality of the space charge effect. The prime objective of the design of MIG is to provide the beam parameters to suffice desired beam-wave interaction in RF structure.

MIG is investigated/evaluated to serve the cyclotron resonance maser and predicted that MIG operation is less sensitive to parameters (except the electric and magnetic field in the cathode region) in limited temperature operation [10], [11]. The megawatt-class relativistic MIG are investigated by Baird *et al.* to serve the 10 GHz gyroklystron amplifier [10]. The design studies of 100 MW MIG has been made through the set of adiabatically approximated trade equations [10], [11], which was further extended and validated with electron trajectory code. Now-a-days, Electron optics (E-gun) is widely employed to study the electron beam propagation in the absence of RF condition. In this section, we have designed and optimised an MIG to improve the performance metrics of the gyro-twystron amplifier.

The propagation of electron beam should support/synchronised with EM wave as well as meet the design expectations of RF interaction structure for efficient beam wave interaction. At the interaction structure, beam parameters such as beam voltage, beam current, pitch factor, velocity spread, guiding centre radius and Larmor radius is chosen to maximise the beam-wave interaction efficiency. The design of the MIG section brings these design parameters to interaction structure by optimising magnetic compression ratio, down taper dimension, cathode slant and cathode-anode gap. In an MIG the guiding centre radius is larger than the radius of Larmor orbit and the electrons are emitted from the cathode, which is generally temperature limited thermionic cathode, in which current variation is easily possible. MIGs are available in two major configurations i.e. single and double anode configurations. The radius of cathode (R_c) is chosen to operate below the electric field breakdown limit ($E_c < 60 \ kV \ /cm$) and the space charge limit ($J_c/J_L < 25 \ \%$). Figure 6.2 (a) shows the variation of electric field, and ratio of current density over the cathode radius and the optimum value of cathode radius is obtained at the intersection

point, 24 mm, at which both system constraints current density ratio and electric field are in the operating limit. From figure 6.2 (a), it can be seen that optimum region of operation is achieved for the cathode radius of 20 mm to 25 mm. Figure 6.2 (b) shows the system constraints (E_c and J_c/J_L) variation over the beam voltage for different radius. From figure 6.2 (b), it can be seen that the optimum value electric field E_c and current density ratio is achieved for the beam voltage from 400 kV to 600 kV.
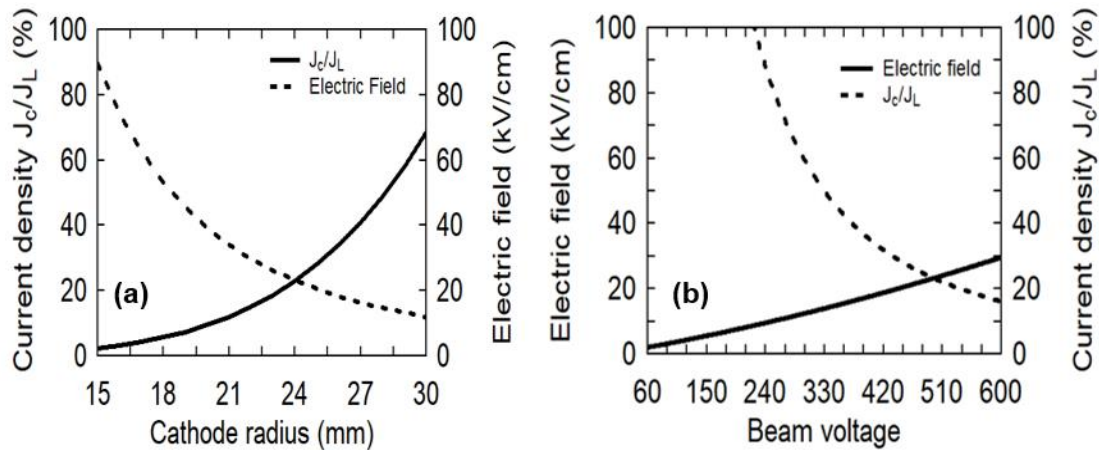

Figure 6.2 Variation of Electric field and the ratio of current density (a) over cathode radius and (b) beam voltage
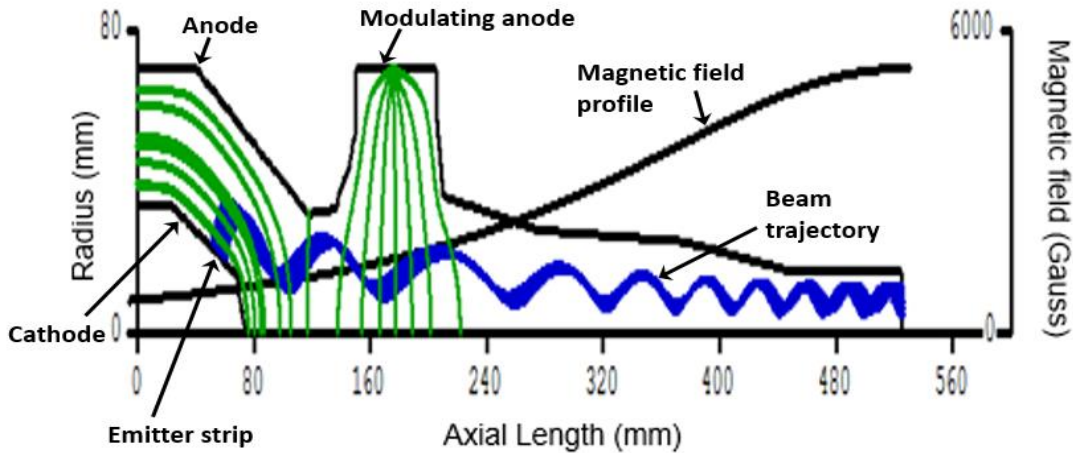

Figure 6.3 Electron beam trajectory in the emitter section

In double anode MIG, the potential at the cathode and the potential difference between the anode and cathode are varied to obtain the desired pitch factor with optimum velocity spread. The electron beam trajectory of double anode MIG is obtained from the E-

gun[112] as shown in the figure 6.3. In figure 6.4 (a), the modulating voltage and beam voltage are varied to achieve the maximum pitch factor with minimum velocity spread. For stable operation, unity pitch factor of electron beam is required in the RF interaction structure. From figure 6.4 (a), it can be seen that below 140 kV of modulating anode voltage, the pitch factor is less than one and the velocity spread shows a linear variation and above 140 kV the pitch factor increases rapidly and the velocity spread shows a nonlinear variation. The unity pitch factor of the electron beam with 3.6 % velocity spread is achieved at 140 kV. Similarly, the beam voltage is varied to optimise the pitch factor and velocity spread. The pitch factor of electron beam decreases with the beam voltage, as the axial component of velocity increases [figure 6.4 (b)]. In this analysis, zero roughness on the emitter surface has been considered; however, the emitter surface roughness of 15 micrometre causes the velocity spread up to 5 % as shown in figure 6.5.
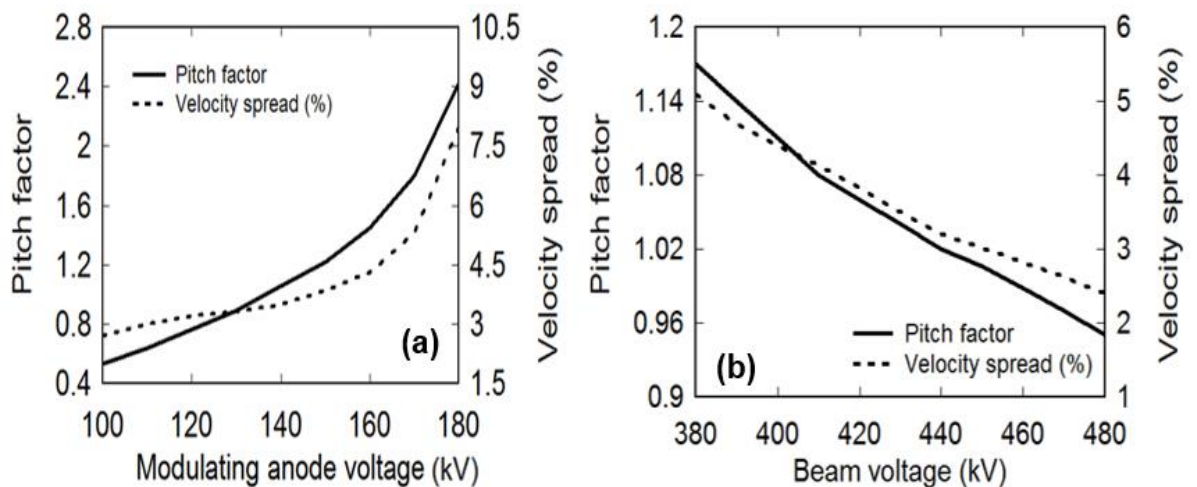

Figure 6.4 Variation of Pitch factor and velocity spread (a) over modulating anode voltage and (b) beam voltage
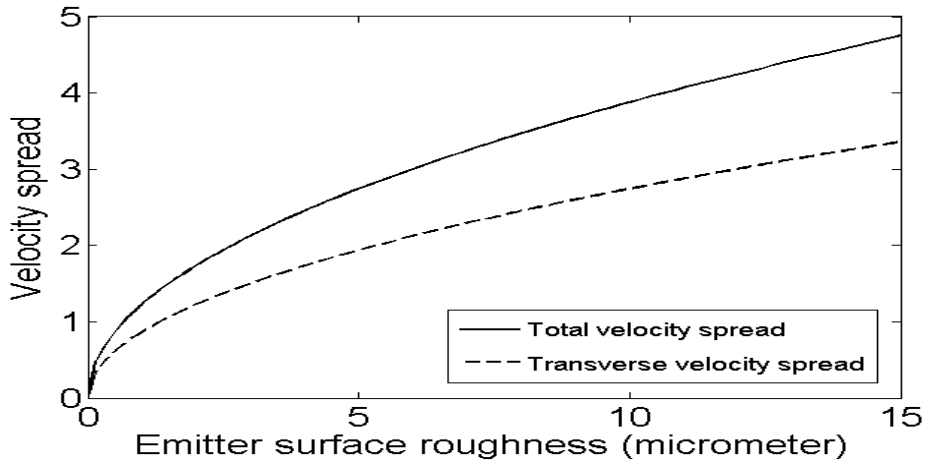
Figure 6.5 Variation of velocity spread over emitter surface roughness

6.2.2 RF Interaction Structure

To achieve the desired goal, the RF interaction structure of two-cavity gyro-twystron is designed to provide an efficient beam-wave interaction and beam parameters are optimised. The radius of the input cavity is chosen such that the cut-off frequency is lower than the operating frequency of an operating mode. The cavity cut-off radius r_{cav} for TE_{mn} mode is given by $r_{cav} = x_{mn}\lambda / 2\pi$, where x_{mn} is an eigenvalue of TE_{mn} mode and λ is a wavelength of RF input signal. The cavities are designed to resonate at the desired frequency and mode. The radius and length of an input cavity are chosen 28.1 mm and 17.3 mm, respectively, to resonate near to 10 GHz in TE_{01} mode, as shown in figure 6.6. The dimension of the second cavity is the slightly different radius, having the radius and length of 28.2 mm and 17.6 mm, respectively. The resonating frequency of 10 GHz is achieved with the further optimisation of dielectric rings. A dielectric ring of BeO-SiC is introduced at the downstream of the metallic cavity to reduce the quality factor and also increase the start oscillation current (SOC). For stable operation of gyro-twystron amplifier, the cavities are operated with the beam current below the SOC. From figure 6.7 (a), it can be seen that an input (first) cavity has higher SOC than the second cavity, as the input cavity has a lower quality factor of 252 than the quality factor 260 of the

second cavity. Figure 6.7 (a) shows that the chosen beam current *(I$_b$ < 200 A)* is well below the SOC for both cavities. The radius of the field-free drift tube is kept 15 mm to provide the cut-off to the operating mode and length is chosen to provide the isolation between field carrying RF structures. The radius and length of drift tube are chosen to provide the isolation by the cold cavity dispersion relation [9].
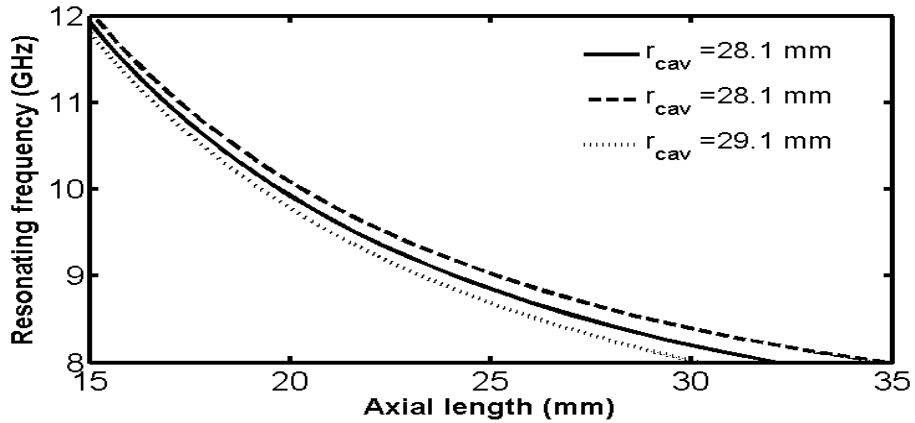

Figure 6.6 Resonating frequency Vs axial length of TE$_{01}$ operated cavity.
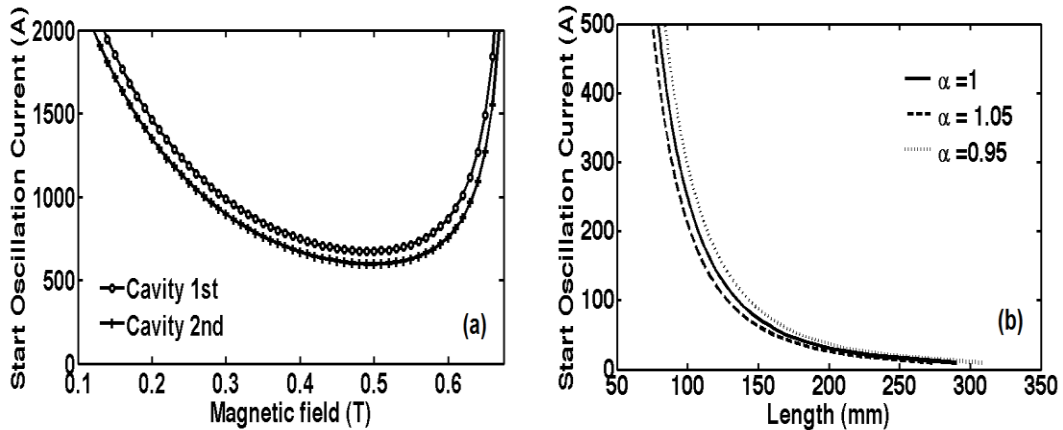

Figure 6.7 SOC Variation of cavities with a magnetic field (b) SOC Vs waveguide length for operating TE$_{01}$ mode.

To attenuate the lower-order mode (other than operating), the dielectric rings are introduced in the drift tube. However, the dielectric ring should start at 1.5 cm away from the cavity [38]. Since the nonlinear beam-wave interaction takes place in the output waveguide, whose length is chosen after the stability analysis [104] and the beam

parameters are chosen carefully to avoid oscillations. Figure 6.7 (b) shows that to operate the device below the SOC of 200 A, the length of the waveguide is kept 100 mm with the assumptions of zero reflectivity. Most importantly, the sensitivity of pitch factor (α=0.95 to 1.05) is incorporated in the calculation of waveguide length [Figure 6.7 (b)] as the exact prediction/measurement of pitch factor is difficult at the waveguide entrance.

Table 6.1 Design parameters of two cavity gyro-twystron

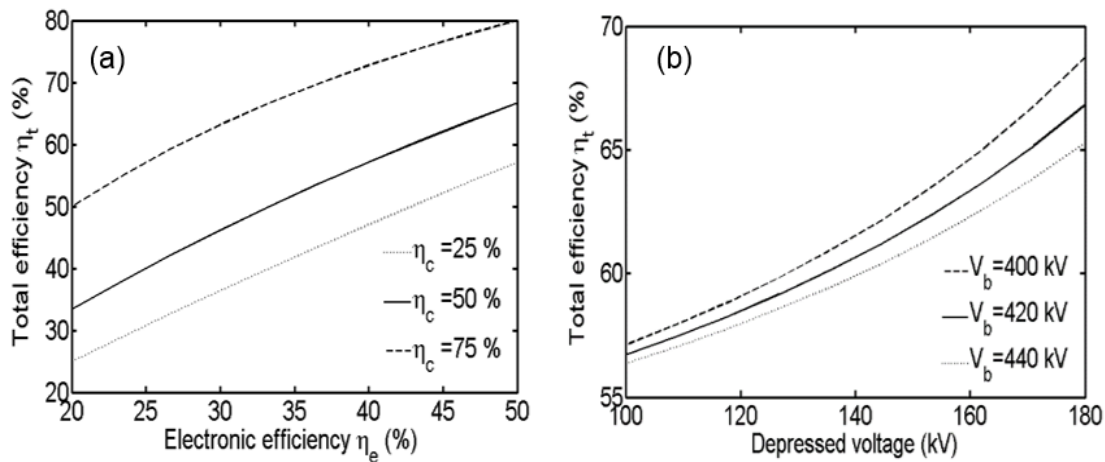| RF subsection	Radius	Length	Particulars	Values
Input cavity	28.1 mm	17.3 mm	Beam voltage	420 kV
First drift tube	15 mm	160 mm	Beam current	180 A
Second cavity	28.2 mm	17.6 mm	Pitch factor	1.0
Second drift tube	15 mm	140 mm	Velocity spread	4 %
Waveguide	19.5 mm	100 mm	RF input power	30 kW

6.2.3 Particle Collector

Figure 6.8 Variation of total efficiency of Gyro-twystron over (a) electronic efficiency and (b) depressed potential
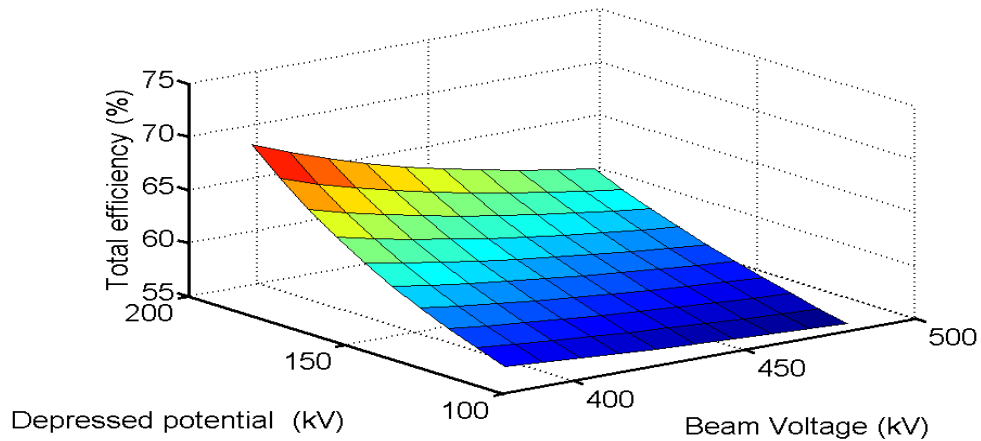
Figure 6.9 Variation of total efficiency of Gyro-twystron over beam voltage and depressed potential
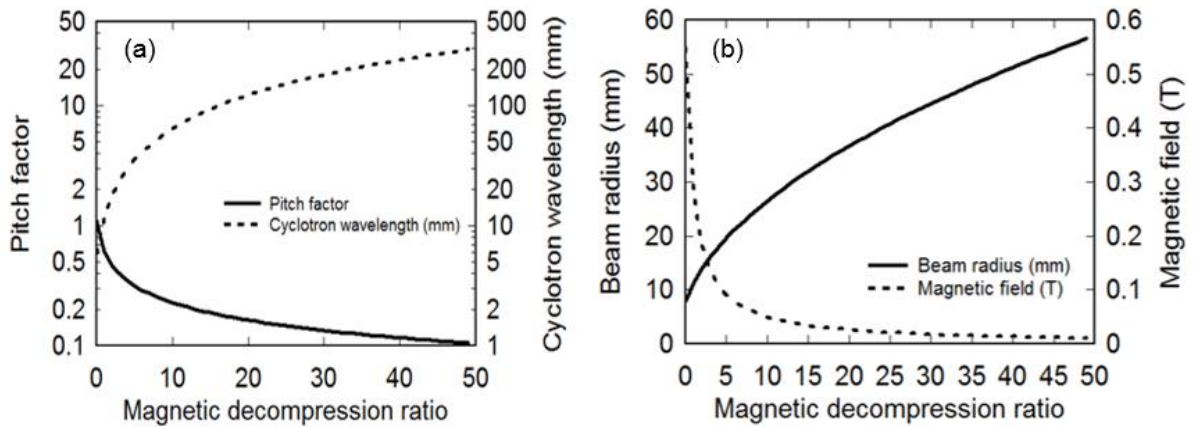

Figure 6.10 Variation of pitch factor and cyclotron wavelength over the magnetic decompression ratio (b) beam radius and magnetic field over the magnetic decompression ratio

The prime motivation behind the design and development of a depressed collector is the efficiency enhancement [113]. From figure 6.8 (a), it can be seen that for the electronic efficiency 40%, the total efficiency of 42 % is achieved with the collector efficiency of 25 %. However, the increased value of total efficiency of 48 % and 70 % has been achieved, for the collector efficiency of 50 % and 75 %, respectively. The improvement in total efficiency of device is primarily dependent on collector efficiency in addition to the electronic efficiency. Figure 6.8 (b) shows that total efficiency of device is increased with depressed potential and efficiency is decreased at higher beam voltage, as the

135

collector efficiency is function of depressed potential of collector electrode and beam voltage. At a beam voltage of 420 kV and 140 kV, the total efficiency of ~59 % is achieved for the electronic efficiency of 39%. Figure 6.8 and 6.9 show that the depressed collector increases the efficiency of gyrotron devices. In gyrotron devices, the majority of electron beam energy is in its transverse motion and to recover the energy of unspent electron beam, perpendicular motion of electron beam is converted into axial motion before applying an electrostatic field to decelerate the electron beam. A large decompression ratio is required to convert the perpendicular energy into axial energy components. The collector beam radius and cyclotron wavelength are primarily dependent on large decompression ratio and determines the dimension of the collector. Figure 6.10 (a) shows that the pitch factor below 0.15 is achieved for a magnetic decompression ratio of 40 and that confirms the maximum energy is in the axial component of electron motion. However, the cyclotron wavelength increases with the decompression ratio at which violates the adiabatic assumption of magnetic decompression. Apart from the magnetic field variation with decompression ratio, figure 6.10 (b) shows an increment of beam radius with the increment of decompression ratio that determines the radius of the depressed collector (60 mm in the present case).

6.3   Beam Wave Interaction Study

6.3.1 Modelling and Cold Simulation

From the calculated design parameters (Table 6.1), the 3D model of two cavity gyro-twystron has been created in CST studio suite, as shown in figure 6.11. Each component is modelled independently to analyse the RF propagation characteristics. The metallic gyro-twystron tube is made of copper (OHFC), having a conductivity of 5.8×10^7 S/m. A dielectric ring of BeO-SiC is introduced at either end of both (first and second) metallic

cavity to achieve the desired quality factor of 252 and 260, respectively. The complex permittivity of BeO-SiC (60%-40%) is 31-13j. The stacks of five dielectric rings are introduced in drift tubes to attenuate the lower order TE_{11} mode. Unlike the prebunching section, the modelling of the output waveguide section is simpler. A hexahedral meshing divides the interaction structure into small solution spaces using a cartesian coordinate system with perfect boundary approximation. The boundary condition is applied to make the tangential electric field zero *(E_t=0)* at the wall of interaction structure. The favourable RF propagation characteristics of each component of gyro-twystron have been ensured using transient solver of CST microwave studio.

1. Particle emitter 2. Predrift tube 3. Input cavity 4. BeO-SiC rings 5. first drift tube
6. second cavity 7. second drift tube 8. taper 9. output waveguide
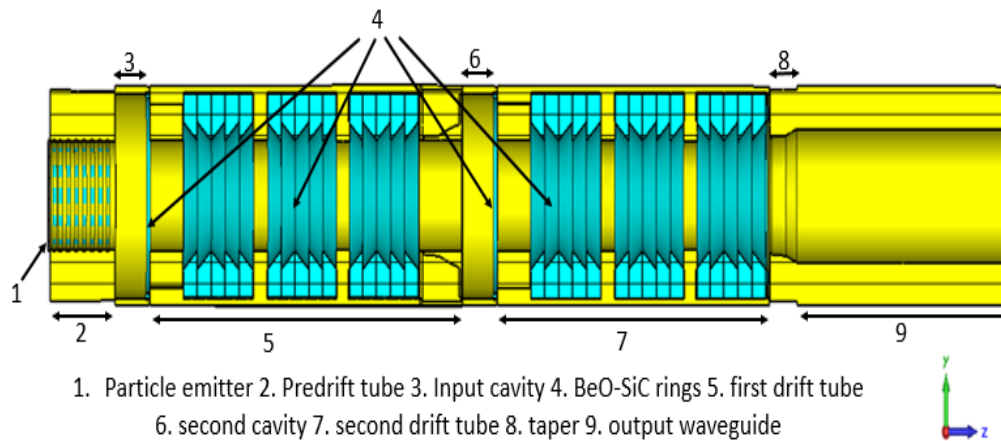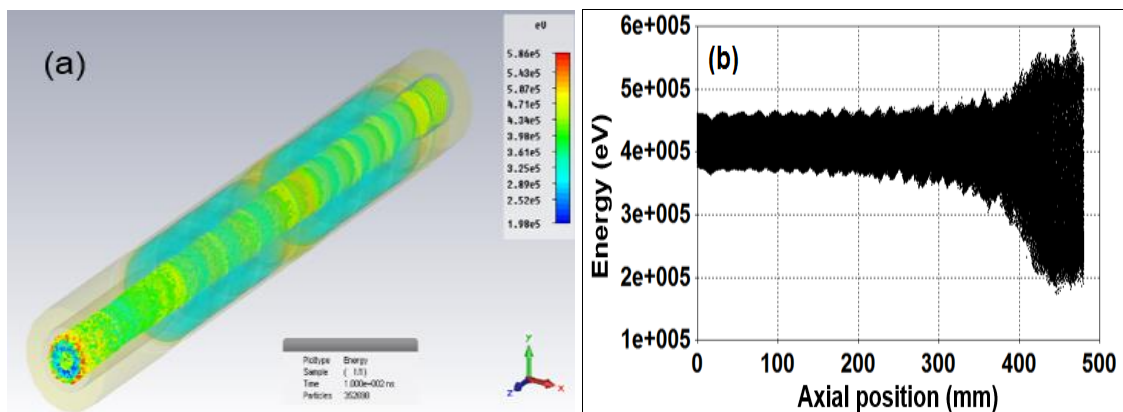
Figure 6.11 CST model of two-cavity gyro-twystron

Figure 6.12 (a) Energy distribution profile of particles in two-cavity gyro-twystron (b) the energy variation along with the axial position.
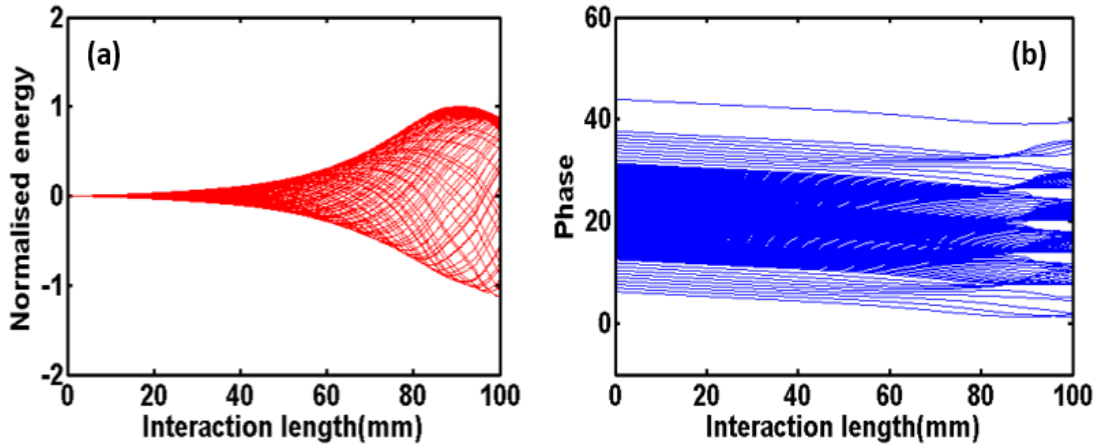
Figure 6.13 Axial variation of (a) normalised energy (b) phase of particles of two-cavity X-band gyro-twystron.
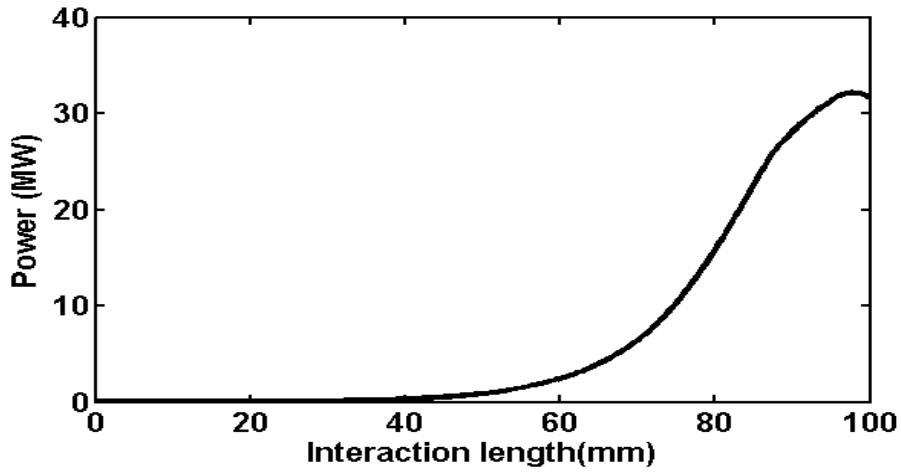

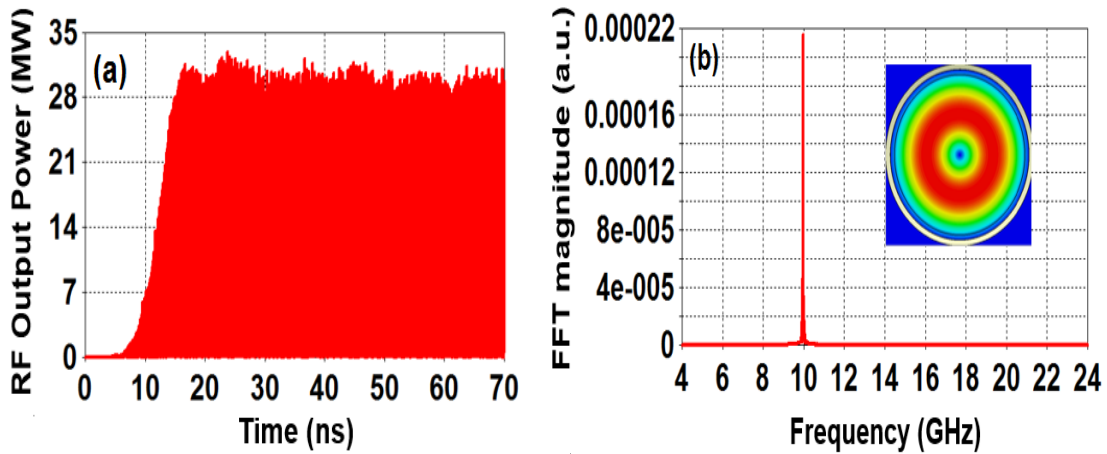Figure 6.14 Axial variation of RF output power in TE_{01} mode.

Figure 6.15 Temporal variation of RF output power (b) the frequency spectrum of two-cavity X-band gyro-twystron

138

6.3.2 PIC Simulation and Validation

3D beam-wave interaction mechanism of X-band two-cavity gyro-twystron has been studied using CST particle studio. The PIC solver incorporated the effect of electron beam and fields on each other in a self-consistent manner. For emitting particles, a cathode is created by a DC emission model of circular particle source. An electron beam 420 kV, 180 A with unity beam velocity pitch factor and 4% spread is considered. Through the predrift tube, electron particles reach the input cavity, where the applied RF input power of 32 kW perturbs particles. These perturbed electrons are ballistically bunched in the first and second drift tube, and prebunched electron beam interacts to RF wave and transferred their energy to RF wave. Figure 6.12 (a) shows the energy of electron along the axial length of gyro-twystron tube, whose profile is represented by the colour ramp. From figure 6.12 (b), it can be seen that electrons with 4% velocity spread, are at a different energy level in the RF interaction structure. As electrons are moving towards the output end of waveguide section, they loose their energy, as shown with lower energy level in figure 6.12 (b). The normalised energy and phase of electrons over the axial length is shown in figure 6.13. Correspondingly, figure 6.14 shows the growth in RF power over the axial length of a waveguide and ~31 MW of RF power is achieved at 100 mm of the waveguide. Figure 6.15 (a) shows that PIC simulation of two-cavity gyro-twystron predicted an RF output power 30 MW in the desired TE_{01} mode. The oscillations in RF output power can be seen as a velocity spread of 4 % is considered in the simulation. The frequency spectrum is shown in figure 6.15 (b), which confirms the output power is developed in TE_{01} mode (inner figure) at 10 GHz. Figure 6.16 shows that the PIC simulation results of two-cavity gyro-twystron are validated using nonlinear theory. The nonlinear theory predicted an RF power of 31.2 MW in TE_{01} mode at 10 GHz and showed a good agreement by 4% with the calculation of PIC simulation. However, far from the

operating frequency, the difference between PIC simulation and nonlinear analysis is increased.
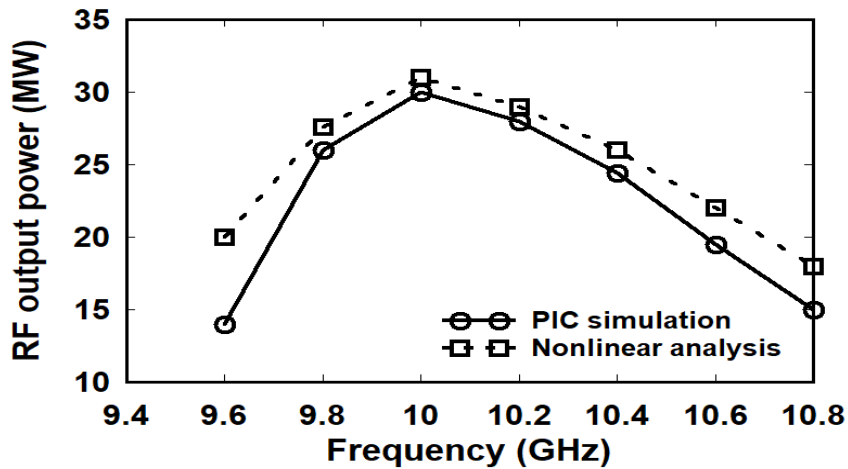

Figure 6.16 Comparison of analytical and PIC simulation RF output power of two cavity gyro-twystron.

6.4   Conclusion

The present chapter discusses the design and simulation of a two cavity gyro-twystron to study its performance improvement by the influence of an introduced intermediate cavity. The single-mode analysis of two-cavity gyro-twystron has predicted ~31 MW of RF power with an efficiency of ~41 % and gain of ~30 dB. These analytical results are validated using 3D PIC code that has predicted ~30 MW of RF power with an efficiency of ~39 % and gain of 29.7 dB. From this study, a significant RF output power and gain improvement has been achieved using additional intermediate cavity. From the analytical and simulation results, it is observed that pre-bunched electron beam provides better growth and saturation of RF power in the short waveguide section of 100 mm. A study on particle emitter suggested that at optimum value of modulating anode voltage of 140 kV, the electron beam with unity pitch factor and 3.6 % spread is achieved. A study on the particle collector suggested that the collecting electrode with a depressed potential of 140 kV, the total efficiency of 59 % is achieved with an electronic efficiency of 39 %.

The studies of particle emitter and collector suggested that the operation at higher modulating voltage and depressed potential can improve the beam-wave interaction efficiency and total efficiency of gyro-twystron, respectively.